CircERBB2IP promotes post-infarction revascularization via the miR-145a-5p/Smad5 axis

Xianping Long,[1,3] Zhimei Qiu,[1,3] Chaofu Li,[1,2,3] Yan Wang,[1] Jiao Li,[1] Ranzun Zhao,[1] Jidong Rong,[1] Ning Gu,[1] Jinson Yuan,[1] Junbo Ge,[2] and Bei Shi[1]

[1]Department of Cardiology, Affiliated Hospital of Zunyi Medical University, Zunyi 563000, China; [2]Department of Cardiology, Zhongshan Hospital, Fudan University, Shanghai, China

Myocardial infarction is one of the leading diseases causing death and disability worldwide, and the revascularization of damaged tissues is essential for myocardial-injury repair. Circular RNAs (circRNAs) are widely involved in physiological and pathological processes in various systems throughout the body, and the role of circRNAs in cardiovascular disease is gaining attention. In this study, we determined that circERBB2IP is highly expressed in the hearts of newborn mice. Silencing or overexpression of circERBB2IP inhibited and promoted angiogenesis _in vivo_ and _in vitro_, respectively. Mechanistically, the transcription factor GATA4 promotes the production of circERBB2IP. Furthermore, circERBB2IP functioned as an endogenous miR-145a-5p sponge and was able to sequester and repress miR-145a-5p activity, which led to an increased expression level of Smad5. In summary, circERBB2IP can promote angiogenesis after myocardial infarction through the miR-145a-5p/Smad5 axis. These data suggest that circERBB2IP may be a potential therapeutic target for the treatment of myocardial infarction.

INTRODUCTION

Coronary artery disease (CAD) is the leading cause of death worldwide.[1] It involves blockage of blood flow to the myocardium, leading to myocardial ischemia or myocardial infarction (MI). Although reperfusion methods such as drug thrombolysis, interventional therapy, or surgical bypass can be used to achieve revascularization, some patients still have insufficient or no myocardial perfusion due to coronary microcirculation dysfunction.[2] The adult mammalian heart has weak regenerative capacity,[3] which is usually insufficient to produce clinically significant myocardial repair subsequent to heart injury. Unlike the adult mammalian heart, the neonatal mouse heart has a high capacity to repair itself in response to injury.[4] Therefore, deconstructing the key molecules and related pathways in the damage and repair of neonatal mice has important implications for improving the prognosis of adult patients with ischemic heart disease.

The non-coding RNA (ncRNA) category, which accounts for 98% of the human transcriptome, is composed of transcripts with multiple functions.[5] Consequently, ncRNAs are critically involved in a wide array of physiological and pathophysiological processes. Circular RNA (circRNA) is a newly discovered endogenous ncRNA.[6] A circRNA is a covalently closed circular molecule, and it lacks both a linear RNA 5′-end cap and a 3′-end polyadenylic-acid structure. It is also not easily degraded by nucleases. With the advancement of high-throughput RNA sequencing technology, a large number of conserved circRNAs have been detected in the heart tissues of humans and rodents.[7] It is considered a key regulator of many physiological and pathological processes in the cardiovascular system. For instance, circSlc8a1 can act as an endogenous sponge for miR-133a in cardiomyocytes to promote pressure-loaded cardiac hypertrophy.[8] In the vascular system, >7,000 circRNAs were identified in endothelial cells, among which the circRNA cZNF292 is capable of promoting angiogenesis _in vitro_.[9] Our previous study also found that cardiomyocytes pre-treated with hypoxia can release circHIPK3-rich exosomes, which regulate the proliferation and apoptosis of endothelial cells under oxidative-stress injury.[10] Nevertheless, there are a large number of circRNAs in the heart whose functions are still unknown and merit further exploration; from the differential screening analysis of circRNA expression profiles between neonatal and adult mouse hearts,[11] we found that circERBB2IP (mmu_circ_0000495) was highly expressed in neonatal mouse hearts and was recently shown to be involved in the proliferation, invasion, angiogenesis, and metastasis of colorectal cancer,[12] but its role in the heart is unknown.

In this study, we found that circERBB2IP was highly expressed in the neonatal mouse heart. In both functional studies of cells and animal experiments, circERBB2IP was found to promote angiogenesis. In
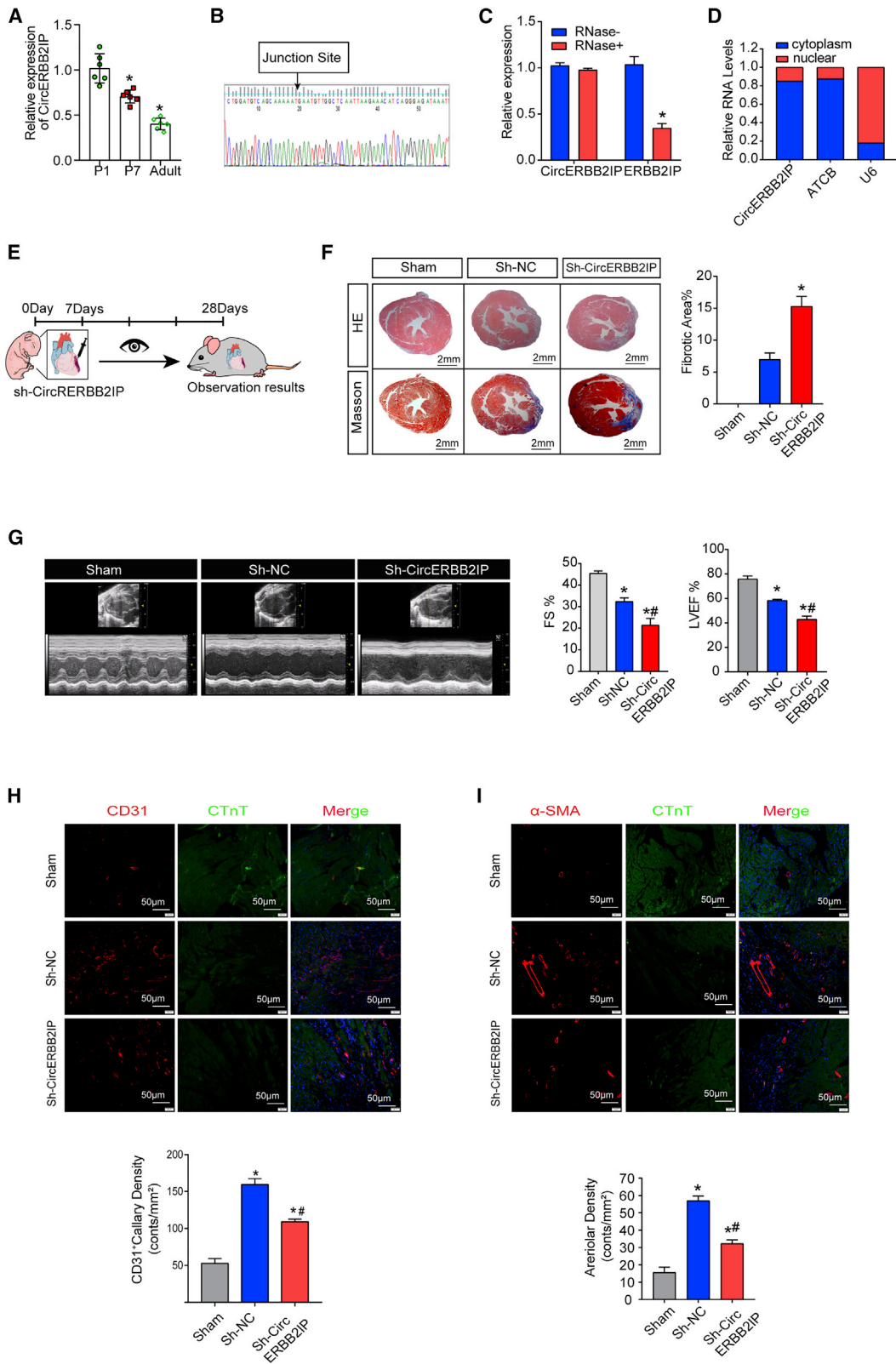
addition, it was shown that circERBB2IP promotes angiogenesis through the miR-145a-5p/Smad5 axis.

RESULTS

circERBB2IP is highly expressed in neonatal hearts, and knockdown of circERBB2IP is detrimental to heart regeneration in newborn mice

ERBB2IP is a member of the leucine-rich repeat sequence and PDZ structural domain protein family and has a protective effect on cardiomyocyte apoptosis under the stimulation of catecholamines,[13] and it has been reported that ERBB2IP can promote angiogenesis.[14] Using the transcriptome dataset reported in a previous study,[11] we analyzed the circRNA expression profiles of neonatal and adult mouse hearts and screened the circRNA circERBB2IP, which is a circRNA containing 364 bases. It is produced by the head-to-tail splicing of exons 2, 3, and 4 of the parental gene ERBB2IP. circERBB2IP was found to be expressed in humans (hsa_circ_0001492) and mice (mmu_circ_0000495) through the circBase database (http://www.circbase.org/). However, the function and effect of circERBB2IP on the heart remain unclear. The expression of circERBB2IP (mmu_circ_0000495) at different time points (post-natal day 1 [P1], P7, adult mice) in heart tissue by qRT-PCR further confirmed that the expression level of circERBB2IP in mouse heart tissue was significantly reduced during the development of the heart, while the expression level of linear ERBB2IP was not significantly altered (Figure 1A and S1A). Sanger sequencing confirmed the specific *trans*-splicing site sequence of circERBB2IP (Figure 1B). In addition, qRT-PCR indicated that circERBB2IP was resistant to RNase R digestion, whereas linear mRNA was easily degraded (Figure 1C). Subsequently, nuclear- and cytoplasmic-separation experiments showed that circERBB2IP was mainly located in the cytoplasm (Figure 1D). We further detected circERBB2IP in several cardiac cell types isolated from neonatal mouse hearts and found that circERBB2IP was mainly expressed in cardiomyocytes and endothelial cells (Figure S1B). It has been reported that differentially expressed circRNAs in neonatal and adult hearts may be involved in heart regeneration. To investigate whether circERBB2IP is also involved in endogenous heart regeneration, P0 mice were treated with adenovirus vector (ADV)-expressing short hairpin RNA (shRNA) targeting circERBB2IP (ADV-shERBB2IP) or negative control (NC) shRNA (ADV-shNC) and subjected to MI through permanent ligation of the left coronary artery (Figure 1E). qRT-PCR assays indicated that ADV-shcircERBB2IP significantly reduced circERBB2IP expression levels in neonatal mouse hearts compared with ADV-shNC (Figure S1C). As expected, knockdown
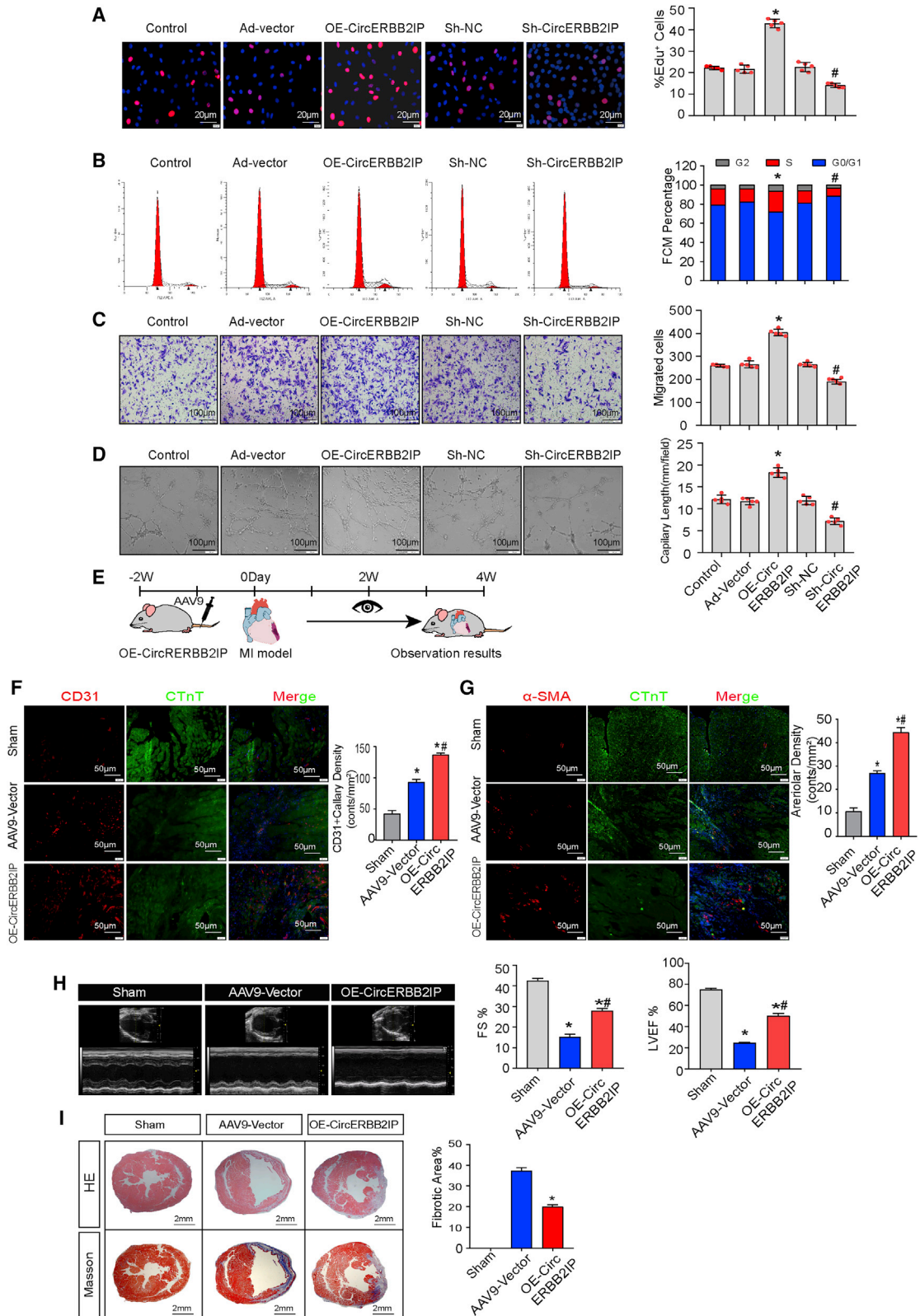
of circERBB2IP significantly increased the scar area of P0 mice after MI, and echocardiography showed that the knockdown of circERBB2IP worsened the heart function of P0 mice (Figures 1F and 1G). The main hazards of MI are the loss of cardiomyocytes and damage to the related vasculature. As expected, the field of cardiac regeneration has focused on the generation of new muscles and blood vessels by targeting cardiomyocyte proliferation and angiogenesis following injury. Consequently, we examined if the knockdown of circERBB2IP affected cardiomyocyte proliferation and angiogenesis. Interestingly, knockdown of circERBB2IP did not reduce the number of phosphohistone H3 (PH3)-positive and Ki67-positive cardiomyocytes (Figures S1D and S1E). We did not find differences in cardiomyocyte (CM) size between circERBB2IP knockdown and NC groups (Figure S1F). Given that knockdown of circERBB2IP had no effect on cardiomyocyte proliferation, we next wanted to determine whether circERBB2IP regulates angiogenesis and found that the number of CD31-positive myocardial capillaries outside in the MI area and the infarct boundary area decreased in circERBB2IP knockdown compared with the ADV control group (Figure 1H). Moreover, we used smooth muscle actin to detect arterioles, and circERBB2IP knockdown also significantly reduced the density of arterioles in the infarcted and infarcted border areas (Figure 1I).

circERBB2IP promotes CMEC proliferation, migration, tube formation, and heart repair after MI in adult mice

Gain-of-function and loss-of-function assays were performed to evaluate the effects of circERBB2IP overexpression and knockdown on the biological behavior of cardiac microvascular endothelial cells (CMECs). CMECs were obtained by enzyme digestion combined with differential adhesion. Immunofluorescence staining showed that the CMECs expressed CD31 and vWF (Figures S2A and S2B). We constructed an adenovirus overexpressing circERBB2IP and designed three shRNAs that knock down circERBB2IP. Results of qRT-PCR showed that the expression of circERBB2IP was significantly up- or downregulated in CMECs transfected with adenovirus or shRNAs, respectively. Neither had any effect on the level of linear ERBB2IP (Figures S2C and S2D). Among the three shRNAs, sh3-circERBB2IP had the highest silencing efficiency; therefore, it was selected for further study. 5-ethynyl-2-deoxyuridine (EdU) and cell-cycle assays were used to detect cell proliferation ability. As shown, the proliferation of CMECs increased after overexpression of circERBB2IP but decreased after circERBB2IP knockdown (Figures 2A and 2B). In addition, Transwell migration and Matrigel

Figure 1. Expression and identification of circERBB2IP and its effect on myocardial infarction in neonatal mice
(A) The expression of circERBB2IP in P1, P7, and adult mouse hearts was detected by qRT-PCR; *p < 0.05 versus adult mice; n = 6. (B) Sanger sequencing verified the back-splice junction sequences and cyclization site of circERBB2IP. (C) Detection of circERBB2IP and ERBB2IP RNA abundance in RNase-R-treated heart tissue by qRT-PCR; *p < 0.05 versus the RNase treatment; n = 4. (D) Cytoplasmic and nuclear RNA-isolation experiments. (E) Schematic diagram of circERBB2IP knockdown after MI in P0 mice and then detecting it at the corresponding time point. (F) Hematoxylin and eosin (H&E) and Masson staining were used to identify the morphology of myocardial tissue in neonatal mice 28 days after MI. Scale bar: 2 mm. *p < 0.05 versus shNC group; n = 6. (G) Cardiac function measured by echocardiography 28 days post-MI (left ventricular ejection fraction, LVEF; fractional shortening, FS). *p < 0.05 versus sham group, #p < 0.05 versus shNC group; n = 6. (H and I) Representative images of capillary density and arterioles measured in the infarct border zone of LV. Capillaries were stained with CD31+ (red, H) and arterioles stained with α-SMA (red, I) myocardium tissue stained with CTnT (green), and nuclei were counterstained with DAPI (blue). Scale bar: 50 μm. *p < 0.05, sham group; #p < 0.05, shNC group; n = 4.

A

B

C

D

E

OE-CircRERBB2IP   MI model   Observation results

F   CD31   CTnT   Merge

G   α-SMA   CTnT   Merge

H   Sham   AAV9-Vector   OE-CircERBB2IP

I   Sham   AAV9-Vector   OE-CircERBB2IP

(legend on next page)

tube-formation assays showed that overexpression of circERBB2IP increased the migration and formation of capillary-like structures in the Matrigel of CMECs, while knockdown of circERBB2IP had the opposite effect (Figures 2C and 2D). Next, to evaluate whether circERBB2IP promotes the angiogenic properties of adult CMECs after MI, we injected AAV9-circERBB2IP and AAV9-Vector through the tail vein and then performed MI surgery in mice (Figure 2E). *In vivo* bioluminescence images and qRT-PCR assays indicated effective vector transduction (Figures S2E and S2F). We found that both capillary and arteriole densities were increased in the border zone of the infarcted hearts at 4 weeks post-MI in mice that received AAV9-circERBB2IP compared with those that received AAV9-control (Figures 2F and 2G). To evaluate whether improved capillary density after MI may improve heart remodeling, we assessed cardiac function by cardiac color Doppler ultrasound and infarct size by Masson's trichrome staining at 4 weeks post-MI in mice. The results showed that compared with the AAV9-Vector group, overexpression of circERBB2IP improved cardiac function and reduced infarct size in mice after MI (Figures 2H and 2I).

GATA4 promotes expression of circERBB2IP

Increasing evidence has indicated that several key transcription factors are involved in the regulation of circRNA.[15] Therefore, we searched for key transcription factors that might be involved in the regulation of circERBB2IP. Using the online transcription-factor-prediction software JASPAR[16] (http://jaspar.genereg.net/), we found 15 putative GATA4- binding sites in the ERBB2IP promoter and selected the two closest binding sites for further study (Figure 3A and S3A). We transfected GATA4 overexpression plasmids or empty vectors into CMECs, and western-blot experiments verified that GATA4 expression was upregulated after transfection (Figure S3B). After that, we constructed a series of luciferase reporter vectors containing the full-length wild-type (WT) or mutant (MUT) ERBB2IP promoter, and dual-luciferase reporter analysis showed that GATA4 promoted the luciferase activity of the WT ERBB2IP promoter but not the MUT ERBB2IP promoter (Figure 3B). We also performed chromatin immunoprecipitation (ChIP)-qPCR assay, and the results showed that GATA4 could bind to the promoter of the ERBB2IP gene and facilitate its transcription activity (Figure 3C). Moreover, transfection of the GATA4 overexpression vector significantly increased circERBB2IP expression levels in CMECs (Figure 3D). These results indicate that the upregulation of circERBB2IP in CMECs may be induced by GATA4.

circERBB2IP directly bind to miR-145a-5p

Previous studies have found that circRNAs located in the cytoplasm may compete with mRNA for the targeted binding site of microRNA (miRNA), thereby regulating mRNA expression. Because circERBB2IP is principally located in the cytoplasm, we determined whether circERBB2IP functions via the same mechanism. Bioinformatics analysis using starBase (http://starbase.sysu.edu.cn/) indicated that miR-145a-5p contains two conserved binding sites for circERBB2IP. miR-145, which has been found to be essential for angiogenesis.[17] Therefore, we further studied the relationship between circERBB2IP and miR-145a-5p. qRT-PCR assays were conducted to investigate the impact of circERBB2IP on the expression of miR-145a-5p. Overexpression or knockdown of circERBB2IP significantly decreased or increased the expression level of miR-145a-5p, respectively (Figure 4A). Next, dual-luciferase reporter assays were performed to measure the binding between circERBB2IP and miR-145a-5p. The psiCHECK2 luciferase reporter plasmid with circERBB2IP WT or MUT-type at the miR-145a-5p binding site was constructed (Figure 4B). The data indicated that miR-145a-5p mimics suppressed the luciferase activity of the psiCHECK2-circERBB2IP-WT luciferase reporter and that the miR-145a-5p inhibitor upregulated the luciferase activity of the psiCHECK2-circERBB2IP-WT luciferase reporter enzyme activity but that it did not affect psiCHECK2-circERBB2IP MUT activity (Figure 4C). In addition, an RNA IP (RIP) assay showed that circERBB2IP and miR-145a-5p were both enriched by AGO2 through the RIP assay (Figure 4D). Furthermore, cytoplasmic and nuclear separation experiments were performed to study the subcellular co-localization of circERBB2IP and miR-145a-5p in CMECs. We found that circERBB2IP and miR-145a-5p were co-localized in the cytoplasm (Figure 4E). Together, these findings suggest that circERBB2IP absorbs miR-145a-5p.

miR-145a-5p inhibits the proliferation, migration, and tube formation of CMECs

Next, we explored the potential role of miR-145a-5p in regulating angiogenesis. miR-145a-5p mimics and miR-145a-5p inhibitors were transfected into CMECs. The results indicated that transfection of miR-145a-5p mimics significantly reduced the proliferation, migration, and tube formation of CMECs. In contrast, transfection of miR-145a-5p inhibitors increased the proliferation, migration, and tube formation of CMECs. These results indicate that miR-145a-5p inhibits the proliferation, migration, and tube formation of CMECs *in vitro* (Figures 5A–5C).

Figure 2. Overexpression of circERBB2IP promotes angiogenesis *in vitro* and *in vivo*

(A and B) Cell proliferation was detected by EdU assay and flow cytometry. Scale bar: 20 μm. *p < 0.05 versus Ad-vector group; #p < 0.05 versus shNC group; n = 5. (C) Migration of CMECs was measured by Transwell migration assays. Scale bar: 100 μm. *p < 0.05 versus Ad-vector group; #p < 0.05 versus shNC group; n = 5. (D) Representative images of CMECs in tube-formation experiment. Scale bar: 100 μm. *p < 0.05 versus Ad-vector group; #p < 0.05 versus shNC group; n = 5. (E) Schematic diagram of MI after circERBB2IP overexpression AAV (OE-circERBB2IP) or control AAV (AAV9-Vector) was injected into the mouse heart via tail vein and then detected at the corresponding time point. (F and G) Representative images of capillary density and arterioles measured in the infarct border zone of LV. Capillaries were stained with CD31+ (red, F) and arterioles stained with α-SMA (red, G) myocardium tissue stained with CTnT (green), and nuclei were counterstained with DAPI (blue). Scale bar: 50 μm. *p < 0.05 versus sham group; #p < 0.05 versus AAV9-Vector group; n = 4. (H) Cardiac function measured by echocardiography 28 days post-MI. *p < 0.05, sham group; #p < 0.05, AAV9-Vector group; n = 6. (I) HE and Masson staining were used to identify the morphology of myocardial tissue in adult mice 28 days after MI. Scale bar: 2 mm. *p < 0.05 versus AAV9-Vector group; n = 6.
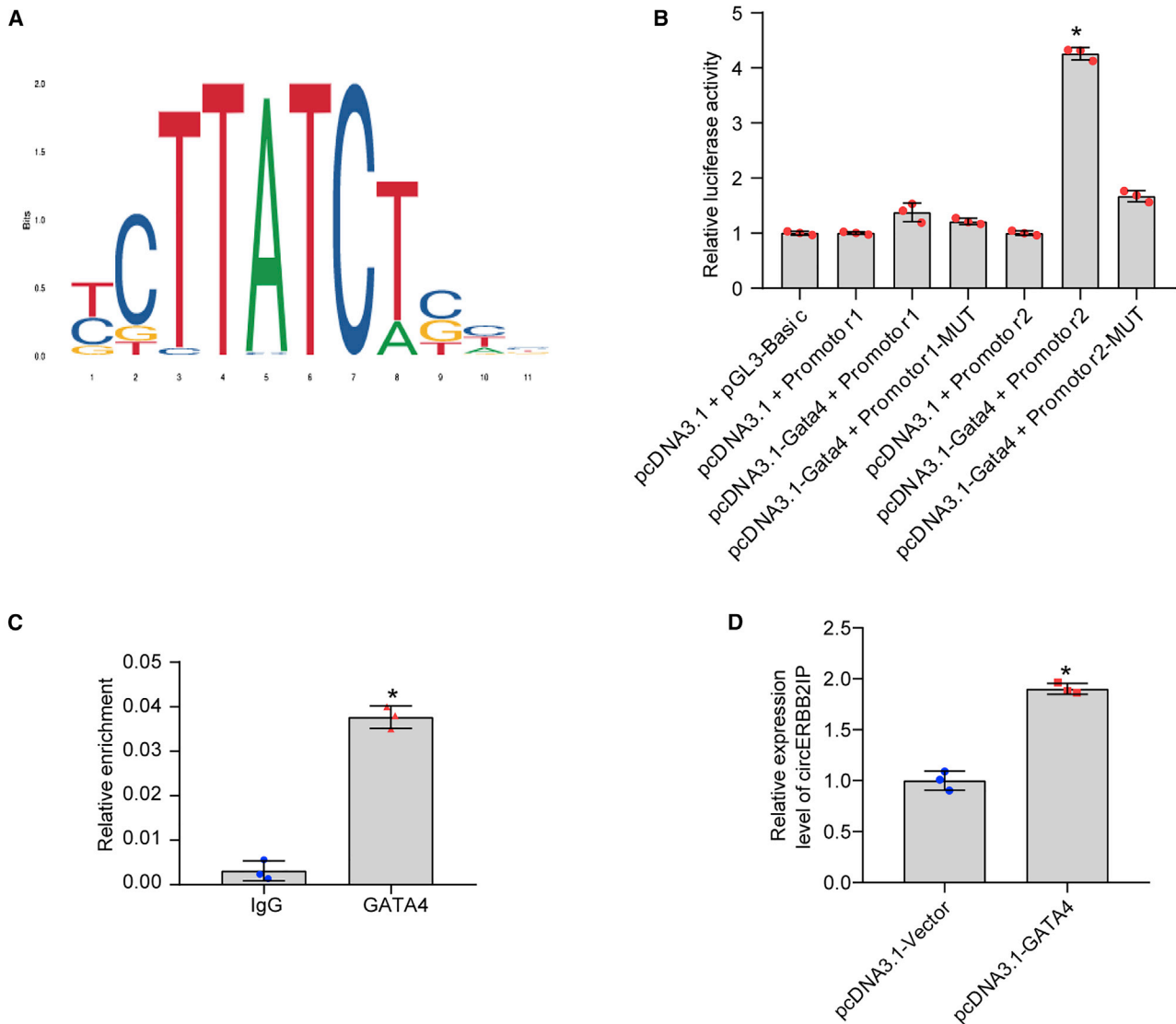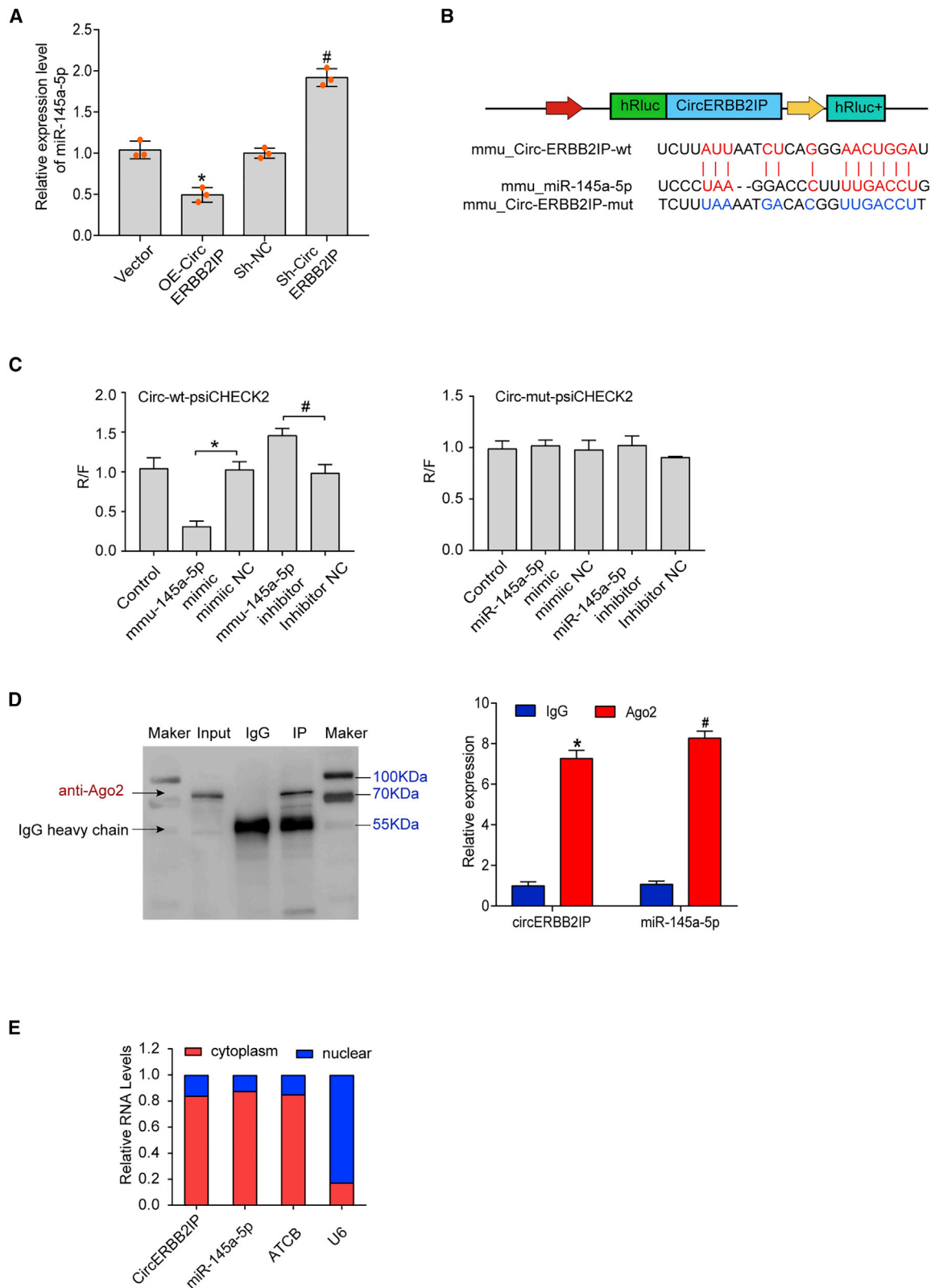
Figure 3. GATA4 promotes expression of circERBB2IP

(A) By using online transcription-factor-prediction software JASPAR, the predicted potential binding sequence logo of GATA4 and circERBB2IP promoter region. (B) Relative luciferase activity was detected in CMECs co-transfected with the luciferase reporter plasmid containing the wild-type or mutant ERBB2IP promoter sequence and the GATA4 overexpression plasmid. *$p < 0.05$ versus mutant ERBB2IP promoter group; n = 3. (C) ChIP-qPCR was performed to analyze the binding of GATA4 to the ERBB2IP promoter. IgG was used as a negative control. *$p < 0.05$ versus IgG group; n = 3. (D) The expression of circERBB2IP was assessed by qRT-PCR in CMECs transfected with a GATA4 overexpression plasmid. *$p < 0.05$ versus pcDNA-vector group; n = 3.

circERBB2IP mediates angiogenesis through circERBB2IP/miR-145a-5p/Smad5 axis

To further determine the downstream target of miR-145a-5p, we used the online tools miRanda (http://www.microrna.org/microrna/home.do) and TargetScan (http://www.targetscan.org/) to predict potential targets of miR-145a-5p. Among them, several molecules of the Smad family have received research interest. Studies have reported that the Smad signaling pathway is involved in cell proliferation and migration and that Smad1/Smad5-mediated signal transduction is necessary for angiogenesis.[18] Bioinformatics analysis indicated that miR-145a-5p may bind to Smad1, Smad3, and Smad5 in the Smad signaling pathway. WT and MUT dual-luciferase reporter plasmids containing Smad1/Smad3/Smad5 3′ untranslated regions (UTRs) were constructed, and the dual-luciferase reporter gene results showed that Smad5 could reduce the luciferase activity, while Smad1 and Smad3 could not (Figure 6A). Western blotting showed that transfection of miR-145a-5p mimics or inhibitors significantly reduced or increased Smad5 protein levels but had no effect on Smad1 and Smad3 protein levels (Figure 6B). Immunofluorescence analysis showed that Smad5 protein was present in both the

A

B


```
mmu_Circ-ERBB2IP-wt     UCUUAUUAATCUCAGGGAACUGGAU
                            | | | |    | |    | | | | | |
mmu_miR-145a-5p         UCCCUAA - -GGACCCUUUUGACCUG
mmu_Circ-ERBB2IP-mut    TCUUUAAAATGACACGGUUGACCUT
```

C

D
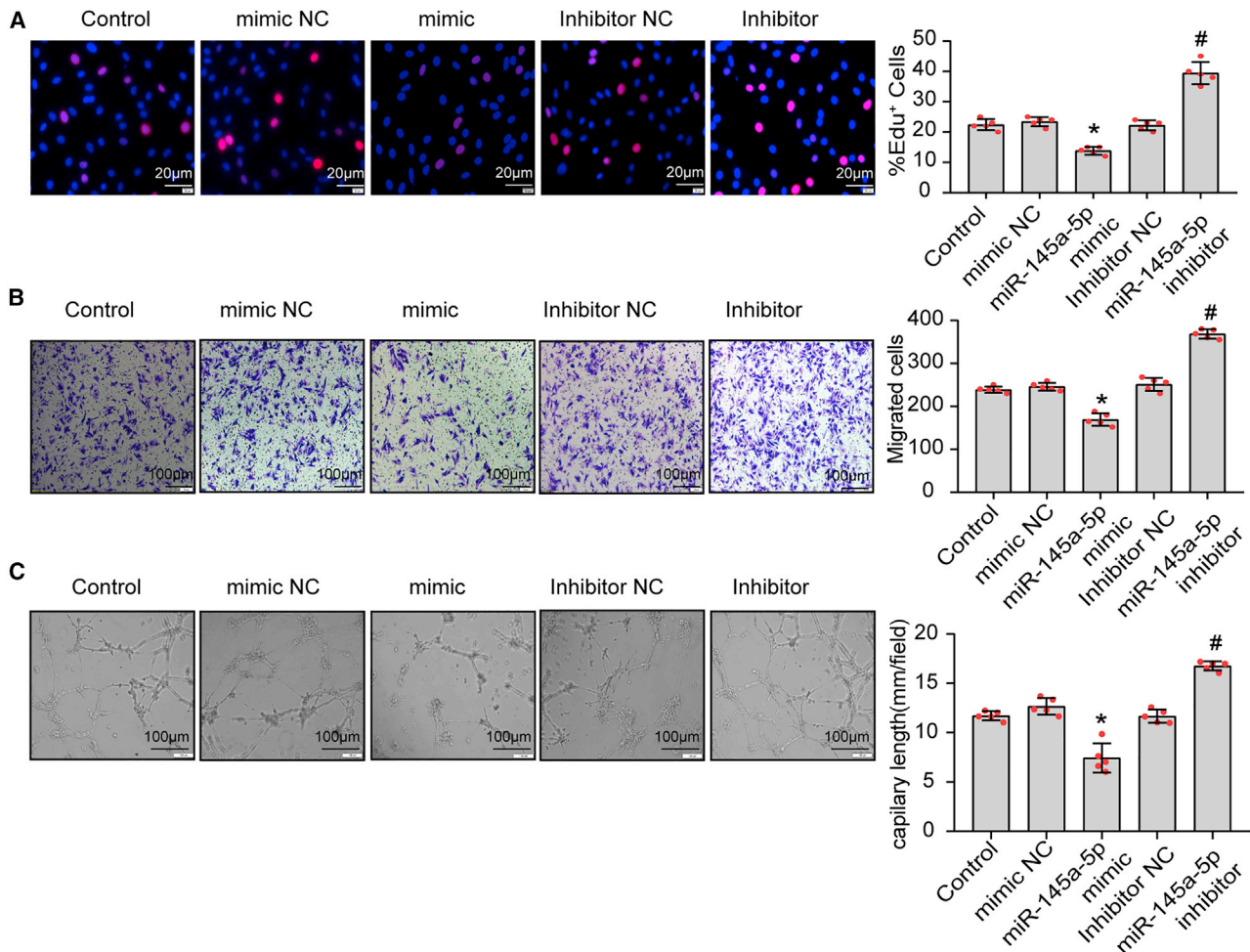

E

(legend on next page)

Figure 5. miR-145a-5p inhibits the proliferation, migration, and tube formation of CMECs

(A) Cell proliferation was detected using the EdU assay. Scale bar: 20 μm. *p < 0.05 versus MNC group; #p < 0.05 versus INC group; n = 5. (B) Transwell migration assay was used to detect the migration ability of CMECs. Scale bar: 100 μm. *p < 0.05 versus MNC group; #p < 0.05 versus INC group; n = 5. (C) Representative images of CMECs in tube-formation experiment. Scale bar: 100 μm. *p < 0.05 versus MNC group; #p < 0.05 versus INC group; n = 5.

cytoplasm and nucleus of CMECs (Figure S4A). These results demonstrate that Smad5 is a direct target of miR-145a-5p.

To further explore the relationship between circERBB2IP, miR-145a-5p, and Smad5, cells were co-transfected with Ad-circERBB2IP and miR-145a-5p mimics. Several rescue experiments were conducted. The results showed that the miR-145a-5p mimic significantly attenuated the proliferation, migration, and tube-formation effects induced by the upregulation of circERBB2IP in CMECs

(Figures 6C–6E). Moreover, western-blotting results revealed that the upregulation of circERBB2IP led to an increase in Smad5 protein levels. miR-145a-5p mimics partially reversed this effect (Figure 6F). In addition, *in vivo* experiments also showed that overexpression of circERBB2IP decreased miR-145a-5p expression and increased Smad5 protein expression levels (Figures S4B and S4C). These results indicate that circERBB2IP increases Smad5 expression level to promote angiogenesis by directly targeting miR-145a-5p.

Figure 4. circERBB2IP directly bind to miR-145a-5p

(A) The expression of miR-145a-5p after up- or downregulation of circERBB2IP was detected by qRT-PCR. *p < 0.05 versus Ad-vector group; #p < 0.05 versus shNC group; n = 3. (B) Schematic diagram shows that circERBB2IP is complementary to the miR-145a-5p seed sequence. (C) The relative luciferase activities were measured in 293 T cells co-transfected with circERBB2IP-WT or circERBB2IP-MUT and miR-145a-5p mimic or miR-145a-5p inhibitor by dual-luciferase reporter gene experiment. *p < 0.05 versus mimic NC (MNC) group; #p < 0.05 versus inhibitor NC (INC) group; n = 3. (D) RIP was performed with an AGO2 antibody in CMECs and then the enrichment of circERBB2IP and miR-145a-5p was detected. (E) The subcellular localization of circERBB2IP and miR-145a-5p were detected by cytoplasmic and nuclear RNA-isolation assay.
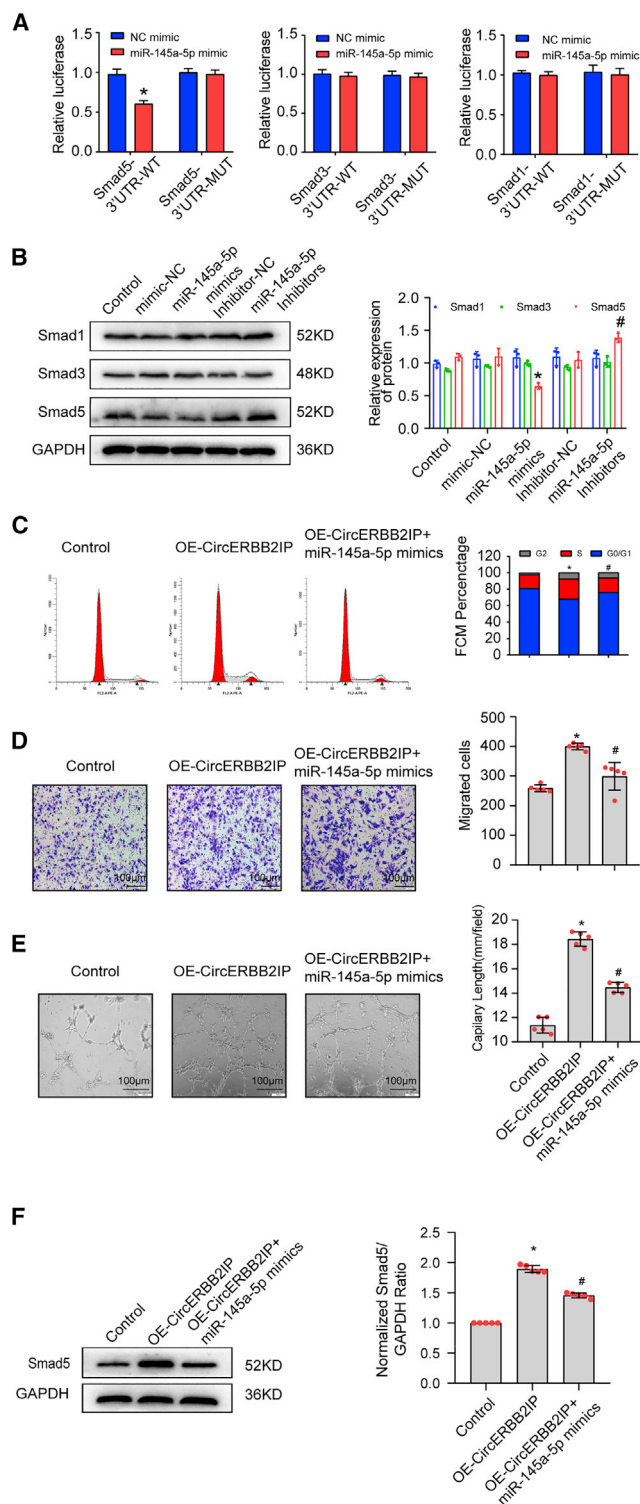
DISCUSSION

MI results in the loss of large numbers of cardiomyocytes and damage to the associated vascular system, and adult mammals have very weak repair ability after heart injury. The difference is that neonatal mice have a powerful self-repair capacity after heart injury. Notably, the growth of new blood vessels produced through angiogenesis was identified as one of the five hallmarks of regeneration.[19] Furthermore, an apical resection model in neonatal mice shows that during cardiac regeneration, endothelial cells first migrate to the thrombogenic region of the apices and then proliferate and migrate to form functional arteries.[20] In addition to supporting cardiomyocytes, revascularization may also guide cardiomyocytes to the injured area. Thus, it is clear that the reconstruction of the vascular network plays an important role in neonatal cardiac regeneration.

circRNA is RNA with a closed loop structure at the 5' and 3' ends that are non-covalently linked an epigenetic new star. They have attracted increasing attention in recent years. RNA sequencing (RNA-seq) has shown that the expression of circRNAs is tissue and developmental-stage specific.[21] Moreover, a large amount of circRNA was found in the heart tissues of mice and humans. This indicates that circRNAs may play an important role in cardiovascular development and diseases, and an increasing number of studies have shown that circRNAs are involved in the regulation of angiogenesis.[22] Therefore, we investigated whether the high expression level of circRNA molecules during the neonatal period is involved in the regulation of angiogenesis.

Here, we screened out circERBB2IP based on the circRNA expression profile of newborn and adult mice. This circRNA is highly expressed in the neonatal heart. Knocking down circERBB2IP is detrimental to cardiac repair after MI in newborn mice. Functionally, we found that knockdown of circERBB2IP inhibited proliferation, migration, and tube formation of CMECs and blocked angiogenesis in the myocardial infarct junctional zone *in vivo*, whereas overexpression of circERBB2IP showed the opposite effect. Intercellular crosstalk synergy is thought to be essential for promoting myocardial capillarization and heart function. We suggest that enhanced neovascularization may be the result of direct action of circERBB2IP on endothelial cells or cellular crosstalk between cardiomyocytes and endothelial cells by paracrine mechanisms. Mechanistically, the transcription factor GATA4 promotes the biogenesis of circERBB2IP. In addition, circERBB2IP acts as a sponge of miR-145a-5p and relieves its inhibitory effect on Smad5. Our data indicate that circERBB2IP could play

Figure 6. circERBB2IP regulates angiogenesis through the circERBB2IP/ miR-145a-5p/Smad5 axis

(A) Luciferase reporter assays showed that miR-145a-5p directly binds to the 3' UTR of Smad5 and inhibits luciferase activity. *p < 0.05 compared with the NC mimics group. (B) The protein-expression levels of Smad1, Smad3, and Smad5 were measured by western blotting. *p < 0.05 versus the MNC group; #p < 0.05 versus the INC group; n = 3. (C) Cell proliferation was detected by flow cytometry. *p < 0.05 versus control group; #p < 0.05 versus OE-circERBB2IP group; n = 5. (D) Transwell migration assay was used to detect the migration ability of CMECs. Scale bar: 100 μm. *p < 0.05 versus control group; #p < 0.05 versus OE-circERBB2IP group; n = 5. (E) Representative images of CMECs in tube-formation experiment. Scale bar: 100 μm. *p < 0.05 versus control group; #p < 0.05 versus OE-circERBB2IP group; n = 5. (F) Smad5 protein expression was detected by western blotting. *p < 0.05 versus control group; #p < 0.05 versus OE-circERBB2IP group; n = 5.
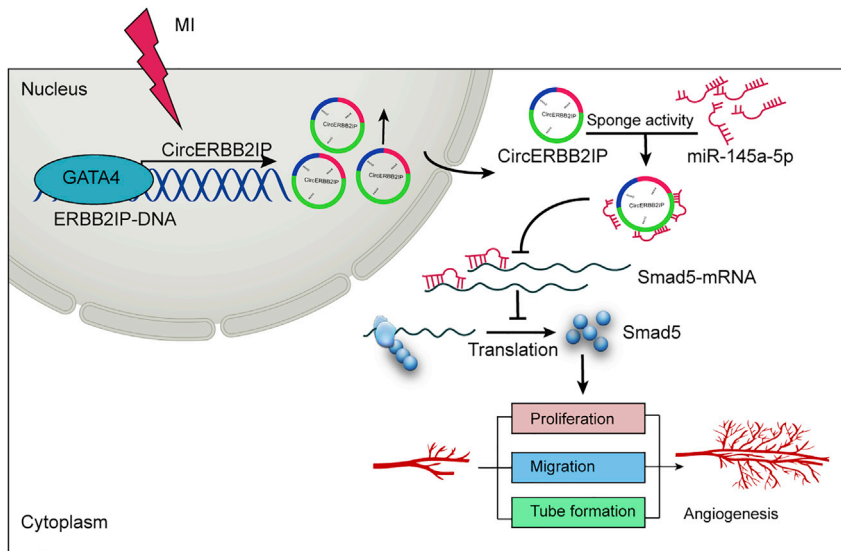
circERBB2IP promotes angiogenesis after myocardial infarction, and *in vitro* experiments have shown that circERBB2IP sponges endogenous miR-145a-5p to isolate and inhibit miR-145a-5p activity, resulting in increased Smad5 expression level, thereby regulating CMEC proliferation, migration, and tubule formation.

an active role in angiogenesis after MI and could be a potential therapeutic target for the treatment of MI.

With the in-depth study of circRNAs, an increasing number of regulatory patterns of circRNA have been revealed. Transcription factors regulate the production of circRNAs. For example, E2F1 promotes the production of circSEPT9 in triple-negative breast cancer.[23] GATA4 is a transcription factor with a conserved zinc-finger domain that regulates cell differentiation and survival, promotes angiogenesis,[24] and improves the function of ischemic myocardium.[25] Bioinformatics analysis predicted that GATA4 could bind to the ERBB2IP promoter, which was confirmed by luciferase reporter gene and ChIP analysis. Subsequently, we found that overexpression of GATA4 increased the expression level of circERBB2IP, suggesting that GATA4 might promote the transcription of circERBB2IP. Therefore, GATA4 may act upstream of circERBB2IP and regulate angiogenesis.

Generally, the cellular location of circRNA determines its function. Through cytoplasmic- and nuclear-isolation experiments, we found that circERBB2IP was mainly located in the cytoplasm. circRNAs located in the cytoplasm mainly exert the effects of miRNA sponges. For example, it was reported that circFAT1 promotes the development of osteosarcoma by binding miR-375 to upregulate the expression of YAP1.[26] By bioinformatics prediction, we found that circERBB2IP could bind many miRNAs, among which it has two binding sites with miR-145a-5p, and studies have reported that miR-145a-p could regulate angiogenesis. Therefore, we hypothesized that circERBB2IP could regulate angiogenesis by binding to miR-145a-5p. qRT-PCR results showed that circERBB2IP and miR-145a-5p share the same subcellular localization in CMECs. Dual-luciferase reporter gene and RIP assays further confirmed that circERBB2IP could bind to miR-145a-5p. These results suggest that circERBB2IP may promote angiogenesis by binding to miR-145a-5p.

Smad family proteins, as mediators of the transforming growth factor-β family, have an important role in transducing signals from the cell surface to the nucleus.[27] In endothelial cells, the TGF-β/Smad signaling pathway plays a bidirectional role in regulating angiogenesis.[28] When TGF-β binds to TβRII, it dimerizes with ALK5, phosphorylates Smad2/Smad3, and activates Smad2/Smad3 and Smad4 to form a heterologous polymer that is transported to the nucleus. This downregulates the expression of angiogenic factors such as vascular endothelial growth factor (VEGF) and inhibits angiogenesis.[29] However, under low tumor growth factor beta (TGF-β) concentrations and hypoxia, TGF-β binds to TβRII and dimerizes with ALK1, activating the Smad1/Smad5/Smad8 signaling pathway, upregulates pro-angiogenic genes, and increases the proliferation and migration of endothelial cells.[30] By bioinformatic prediction, we found that Smad1/Smad3/Smad5 of Smad family proteins might bind to miR-145a-5p. Further, through luciferase gene reports and western-blot experiments, we found that Smad5 may bind to miR-145a-5p. Studies have shown that mice with homozygous mutations of Smad5 died at day 10.5 to 11.5 of gestation due to defective angiogenesis. In addition, Smad5 plays an important role in early post-natal retinal angiogenesis and remodeling.[31] Smad5 plays an important role in angiogenesis. Our study showed that the expression of Smad5 protein was upregulated when circERBB2IP was upregulated. This effect was partially reversed by the addition of miR-145a-5p. These results indicate that circERBB2IP binds miR-145a-5p through a competitive endogenous RNA mechanism and upregulates the expression of Smad5 to promote angiogenesis.

The present findings provide evidence that circERBB2IP is highly expressed in the neonatal mouse heart. circERBB2IP promotes post-infarction neovascularization as well as the proliferation, migration, and tube formation of CMECs cultured *in vitro*. Mechanistically, circERBB2IP promotes angiogenesis through the circERBB2IP/miR-145a-5p/Smad5 axis. Furthermore, we demonstrated that GATA4 mediates the biogenesis of circERBB2IP (Figure 7). Therefore, our data suggest that circERBB2IP may be a potential therapeutic target for the treatment of MI.

MATERIALS AND METHODS
Animals
C57BL/6J mice were purchased from the Zunyi Medical University. Animal care, surgery, and handling procedures were approved by

the Institutional Animal Care and Use Committee of the University of Zunyi Medical University. The study was approved by the Medical Ethics Committee of Zunyi Medical University (approval number: KLLY(A)-2020-011).

Isolation and culture of cardiac endothelial cells

CMECs were isolated from post-natal C57BL/6J mice according to a previously published protocol.[32] In summary, the mice were euthanized and immersed in 75% alcohol. The chest was opened to extract the heart, atrium, connective tissue, fat, and blood vessels. Next, the ventricular tissue was cut into small pieces and digested with 0.08% trypsin and 0.1% collagenase II at 37°C under stirring for 40 min. The supernatant was transferred to a 50-mL centrifuge tube containing 10% fetal bovine serum (FBS) Dulbecco's modified Eagle's medium (DMEM) to terminate the detachment. The digested solution was filtered through a 200-mesh sieve and centrifuged at 1,200 RPM for 5 min at room temperature. The supernatant was discarded, and the cell pellet was resuspended in DMEM containing 10% FBS and placed in a 5% carbon dioxide incubator at 37°C for 1 h to separate cardiac fibroblasts. The non-adherent cell suspension was centrifuged at 1,200 RPM for 5 min, the supernatant was discarded, and endothelial cell-culture medium (ECM; Procell, Austin, TX, USA) was added to resuspend the cell pellet and placed in a poly lysine pre-coated culture flask to continue culturing. After 48 h, the cell-culture medium was changed, and cell growth was observed under a microscope.

Establishment of MI model

P0 mice were placed on ice for 5–8 min to induce anesthesia, and adult mice were anesthetized by inhalation of 2% isoflurane. After disinfection, the skin was cut off between the third and fourth ribs on the left edge of the sternum. The pectoralis major and external intercostal muscles were blunt separated. The intercostal space was pierced with curved hemostatic forceps between the third and fourth ribs. Immediately after, the left thumb and index finger were quickly removed from the heart. The left anterior descending artery (LAD) coronary artery was ligated with 8.0/5.0 needle sutures. Similar operations were performed without ligation in the sham-operated group.

Echocardiography

Heart function was examined by echocardiography using a Vevo 2100 ultra-high-resolution small animal imaging system (VisualSonics, Toronto, ON, Canada). Four weeks after MI, the mice were anesthetized with a mixture of 1.5% isoflurane and oxygen (1 L/min), and left ventricular ejection fraction (LVEF) and fractional shortening (FS) were calculated using the corresponding formulas as described previously.

Histological examinations

Fresh heart tissue was fixed with 4% paraformaldehyde for 24 h, embedded in paraffin, and sectioned. The sections were deparaffinized sequentially with xylene and gradient ethanol, and the Masson Trichrome Staining Kit (Solarbio, Beijing, China, G1346) and hematoxylin and eosin staining kit were used to detect fibrotic areas per the

manufacturer's instructions. The area of MI fibrosis was measured using the ImageJ software.

Immunofluorescence analysis

Fresh heart tissue was embedded and sliced using optimal cutting temperature (OCT). Tissue sections and cultured cells were fixed in 4% paraformaldehyde for 30 min and then permeabilized with 1% Triton X-100 in PBS for 10 min. The samples were incubated with goat serum at room temperature for 1 h. Afterward, the samples were incubated overnight at 4°C with the following primary antibodies, which were diluted with goat serum: anti-cardiac troponin T (cTnT; ab8295; Abcam, Cambridge, UK), anti-pH3 (53348; CST, Danvers, MA, USA), anti-Ki67 (ab15580; Abcam), anti-α-SMA (ab124964; Abcam), and anti-CD31 (ab222783; Abcam). The next day, the samples were stained with fluorescent secondary antibodies (Alexa Fluor 488 and/or 594; Proteintech, Rosemont, IL, USA) at room temperature for 1 h. The nuclei were stained with 4, 6-diamino-2-phenylindole (DAPI; Sigma-Aldrich, St. Louis, MO) for 10 min. Images were collected using a fluorescence microscope (Olympus, Tokyo, Japan).

EdU proliferation assay

Cell proliferation was detected using Cell-light EdU Apollo 567 *in vitro* kit (RiboBio, Guangzhou, China) according to the manufacturer's instructions. First, cells were incubated in EdU medium for 2 h. Next, the cells were fixed in 4% paraformaldehyde at room temperature for 30 min and stained with Apollo staining solution for 30 min, and nuclei were stained with Hoechst 33342. Images were captured using a fluorescence microscope (Olympus).

Cell-cycle assay

The cells were collected and fixed in 70% cold ethanol for 24 h. Propidium iodide (PI) staining solution was used for staining at 37°C for 30 min, and the samples were analyzed by flow cytometry (Millipore Guava, Burlington, MA, USA).

Transwell migration assay

One-hundred μL CMECs cell suspension (1×10^5 cells) was added to a Transwell chamber (3422, CoStar, Washington, DC., USA), and 600 μL complete medium was added into the lower chamber. Transwell inserts were incubated in an incubator at 37.5°C and 5% CO2 for 24 h. Non-migrated cells in the upper chamber were gently wiped off with cotton swabs, and the chamber was washed with PBS, fixed with 4% paraformaldehyde for 30 min, and then stained with 1% crystal violet for 15 min. Five random fields of view were photographed and counted under an inverted microscope.

Tube-formation experiment

Matrigel (BD, Franklin Lakes, NH, USA) was melted in a 4°C refrigerator in advance, and 50 μL of Matrigel was added to a 48-well plate with a pre-cooled pipette gun. The 48-well plate was placed in a 37°C incubator for 45 min to solidify the Matrigel. Then, 150 μL cell suspension (2×10^5 cells) was added and seeded on the surface of Matrigel and incubated in an incubator at 37°C for 6 h. The images were

captured under a microscope, and tube formations were analyzed using ImageJ software.

Luciferase reporter assay

The circERBB2IP (psiCHECK2-circ-0000495) or Smad5 3' UTR (psiCHECK2-smad5 3' UTR) sequences containing the WT or MUT binding site of miR-145a-5p were designed and synthesized by GeneSeed (Guangzhou, China). To construct the luciferase reporter gene vector containing the ERBB2IP promoter, the ERBB2IP promoter containing WT and MUT was cloned into the pGL3 basic vector (Genecreate, Wuhan, China) and co-transfected with GATA4 empty vector or overexpression vector. After 48 h of incubation, the dual-luciferase reporter gene detection kit (Promega, USA) was used for detection per the manufacturer's instructions.

ChIP assay

Cells were crosslinked with 1% formaldehyde for 10 min, terminated with 125 mM glycine, and washed with pre-cooled PBS. The cell pellet was resuspended in IP lysate containing a protease inhibitor and lysed on ice for 30 min. Next, the DNA-protein complex was treated with an ultrasound to produce 200–1,000-bp DNA fragments. Anti-GATA4 antibody (Thermo Fisher Scientific, Waltham, MA, USA) was added to form an antibody-target protein-DNA complex overnight at 4°C, and then protein A + G agarose was used for IP. After washing and reverse crosslinking, free DNA was obtained. The DNA was purified using a spin column and examined by qRT-PCR.

RIP

RIP assays were performed using the Magna RIP RNA-Binding Protein Immunoprecipitation Kit (Millipore, Billerica, MA, USA) according to the manufacturer's protocol. Cells were collected and lysed in RIP lysis buffer and incubated with magnetic beads conjugated with an anti-Argonaute 2 (Millipore) or NC anti-IgG (Millipore) antibody for 6 h at 4°C. Samples were washed with RIP wash buffer and incubated with proteinase K to remove proteins, and purified RNA was analyzed by qRT-PCR.

RNA extraction, nuclear-cytoplasmic fractionation, RNase R, and qRT-PCR assays

Total RNA was isolated from tissues or cells using TRIzol reagent (Takara, Dalian, China). Cytoplasmic and nuclear RNA were isolated from cells using cytoplasmic and nuclear RNA extraction kits (Norgen Biotek, Thorold, ON, Canada) per the manufacturer's instructions. RNase R therapy was performed according to a previously described protocol.[10] In summary, approximately 2 µg total RNA was treated with or without 3 µg RNase R (Epicenter Technologies, Madison, WI, USA) at 37°C for 30 min. RNA was reverse transcribed into cDNA using the PrimeScript RT Kit (Takara) according to the manufacturer's instructions. The sequences of primers for quantitative real-time RT-PCR were as follows: circERBB2IP-F 5'-CTGGATGTCAGCAAAAATGAATGTT-3' and circERBB2IP-R 5'-TCGTAGACAGCGACATGGTA-3'; ERBB2IP-F 5'-TTTGTTG AGCAGGAGGGCCA-3' and ERBB2IP-R 5'-TCTACCGAAACGA

CCTCCGC-3'; GAPDH-F 5'-GGTTGTCTCCTGCGACTTCA-3' and GAPDH-R 5'-TGGTCCAGGGTTTCTTACTCC-3'; ATCB-F 5'-GTGCTATGTTGCTCTAGACTTCG-3' and ATCB-R 5'-ATGC CACAGGATTCCATACC-3'; U6-RT 5'-GTCGTATCCAGTGCA GGGTCCGAGGTATTCGCACTGGATACGACAAAAT-3'A, U6-F 5'-AGAGAAGATTAGCATGGCCCCTG-3' and U6-R 5'-ATCC AGTGCAGGGTCCGAGG-3';

miRNA was reverse transcribed with miRNA-specific stem-loop primers. The relative gene-expression levels were quantified using the $2^{-\Delta\Delta Ct}$ method.

Western blot

The protein was extracted and quantitated. The identical quantity of protein was separated by 12% SDS-PAGE gels and transferred to PVDF membranes (Millipore). The membrane was sealed with 5% skim milk and incubated with primary antibody against. They were then incubated with HRP-conjugated secondary antibody at room temperature for 1 h. Protein signals were assessed by an enhanced chemiluminescence (ECL) reagent on a ChemiDoc MP system. The grayscale value of the target band was analyzed using ImageJ software.

Plasmid, ADV, AAV9, and vector transfection

The ADV and adeno-associated virus serotype 9 (AAV9) vectors for circERBB2IP overexpression or knockdown were synthesized by Hanbio (Shanghai, China). pcDNA3.1-GATA4 and pcDNA3.1-empty vectors were purchased from General Biosystems (Anhui, China). miR-145a-5p mimics, inhibitors, and NCs were obtained from RiboBio. Transfection was performed using Lipofectamine 3000 (Invitrogen, Waltham, MA, USA) according to the manufacturer's instructions. At 48 h after transfection, qRT-PCR was performed to evaluate gene expression. Briefly, mice were injected with AAV9 virus into the tail vein 2 weeks prior to MI surgery, which was performed by ligating the anterior descending branch of the left coronary artery. Myocardial tissues were collected 28 days after injection. In P0 newborn mice, ADV-shcircERBB2IP or ADV-shNC were injected into three sites (one injection at the ligation point, and one injection on each side of the sector) in the left ventricle by using an insulin syringe with a 31G needle.

STATISTICAL ANALYSIS

Statistical analysis was mainly performed by the SPSS 21.0 statistical software package (IBM, Armonk, NY, USA) and GraphPad Prism 7.0 (GraphPad Software, San Diego, CA, USA). The data were normally distributed and expressed as mean ± SD. One-way analysis of variance (ANOVA) was used to compare multiple groups. In addition, p values less than 0.05 were considered statistically significant.

SUPPLEMENTAL INFORMATION

Supplemental information can be found online at https://doi.org/10. 1016/j.omtn.2022.04.006.

ACKNOWLEDGMENTS

AUTHOR CONTRIBUTIONS

B.S., J.G., and Z.Q. conceived and designed this study; X.L., C.L., and Z.Q. performed most of the experiments; Y.W., R.Z., and J.L. analyzed the date; C.L., J.R., N.G., and J.Y. prepared figures; Z.Q. and X.L. drafted the paper; B.S. revised the paper.

DECLARATION OF INTEREST

The authors declare that there is no conflict of interest regarding the publication of this article.

REFERENCES

1. Virani, S.S., Alonso, A., Benjamin, E.J., Bittencourt, M.S., Callaway, C.W., Carson, A.P., Chamberlain, A.M., Chang, A.R., Cheng, S., Delling, F.N., et al. (2020). Heart disease and stroke statistics-2020 update: a report from the American heart association. Circulation 141, e139–e596. https://doi.org/10.1161/cir.0000000000000757.

2. Wu, X., Reboll, M.R., Korf-Klingebiel, M., and Wollert, K.C. (2021). Angiogenesis after acute myocardial infarction. Cardiovasc. Res. 117, 1257–1273. https://doi.org/10.1093/cvr/cvaa287.

3. Bergmann, O., Bhardwaj, R.D., Bernard, S., Zdunek, S., Barnabé-Heider, F., Walsh, S., Zupicich, J., Alkass, K., Buchholz, B.A., Druid, H., et al. (2009). Evidence for cardiomyocyte renewal in humans. Science 324, 98–102. https://doi.org/10.1126/science.1164680.

4. Porrello, E.R., Mahmoud, A.I., Simpson, E., Hill, J.A., Richardson, J.A., Olson, E.N., and Sadek, H.A. (2011). Transient regenerative potential of the neonatal mouse heart. Science 331, 1078–1080. https://doi.org/10.1126/science.1200708.

5. Bär, C., Chatterjee, S., Falcão Pires, I., Rodrigues, P., Sluijter, J.P.G., Boon, R.A., Nevado, R.M., Andrés, V., Sansonetti, M., de Windt, L., et al. (2020). Non-coding RNAs: update on mechanisms and therapeutic targets from the ESC working groups of myocardial function and cellular biology of the heart. Cardiovasc. Res. 116, 1805–1819. https://doi.org/10.1093/cvr/cvaa195.

6. Kristensen, L.S., Andersen, M., Stagsted, L.V.W., Ebbesen, K.K., Hansen, T.B., and Kjems, J. (2019). The biogenesis, biology and characterization of circular RNAs. Nat. Rev. Genet. 20, 675–691. https://doi.org/10.1038/s41576-019-0158-7.

7. Xia, S., Feng, J., Lei, L., Hu, J., Xia, L., Wang, J., Xiang, Y., Liu, L., Zhong, S., Han, L., and He, C. (2017). Comprehensive characterization of tissue-specific circular RNAs in the human and mouse genomes. Brief. Bioinform. 18, 984–992. https://doi.org/10.1093/bib/bbw081.

8. Lim, T.B., Aliwarga, E., Luu, T.D.A., Li, Y.P., Ng, S.L., Annadoray, L., Sian, S., Ackers-Johnson, M.A., and Foo, R.S.Y. (2019). Targeting the highly abundant circular RNA circSlc8a1 in cardiomyocytes attenuates pressure overload induced hypertrophy. Cardiovasc. Res. 115, 1998–2007. https://doi.org/10.1093/cvr/cvz130.

9. Boeckel, J.N., Jaé, N., Heumüller, A.W., Chen, W., Boon, R.A., Stellos, K., Zeiher, A.M., John, D., Uchida, S., and Dimmeler, S. (2015). Identification and characterization of hypoxia-regulated endothelial circular RNA. Circ. Res. 117, 884–890. https://doi.org/10.1161/circresaha.115.306319.

10. Wang, Y., Zhao, R., Liu, W., Wang, Z., Rong, J., Long, X., Liu, Z., Ge, J., and Shi, B. (2019). Exosomal circHIPK3 released from hypoxia-pretreated cardiomyocytes regulates oxidative damage in cardiac microvascular endothelial cells via the miR-29a/IGF-1 pathway. Oxid. Med. Cell. Longev. 2019, 7954657. https://doi.org/10.1155/2019/7954657.

11. Werfel, S., Nothjunge, S., Schwarzmayr, T., Strom, T., Meitinger, T., and Engelhardt, S. (2016). Characterization of circular RNAs in human, mouse and rat hearts. J. Mol. Cell. Cardiol. 98, 103–107. https://doi.org/10.1016/j.yjmcc.2016.07.007.

12. Chen, L.Y., Wang, L., Ren, Y.X., Pang, Z., Liu, Y., Sun, X.D., Tu, J., Zhi, Z., Qin, Y., Sun, L.N., and Li, J.M. (2020). The circular RNA circ-ERBIN promotes growth and metastasis of colorectal cancer by miR-125a-5p and miR-138-5p/4EBP-1 mediated cap-independent HIF-1α translation. Mol. Cancer 19, 164. https://doi.org/10.1186/s12943-020-01272-9.

13. Shi, M., Zhao, M., Hu, M., Liu, D., Cao, H., Qian, L., Yang, Z., Hu, Y., Yu, M., Yang, S., et al. (2013). β2-AR-induced Her2 transactivation mediated by Erbin confers protection from apoptosis in cardiomyocytes. Int. J. Cardiol. 167, 1570–1577. https://doi.org/10.1016/j.ijcard.2012.04.093.

14. Jin, X., Li, B., Zhao, Y., Liu, X., Li, Y., Song, L., Cui, L., Xie, D., Li, T., Zhang, X., and Guo, Y. (2019). Erbin plays a critical role in human umbilical vein endothelial cell migration and tubular structure formation via the Smad1/5 pathway. J. Cell. Biochem. 120, 4654–4664. https://doi.org/10.1002/jcb.27754.

15. Meng, J., Chen, S., Han, J.X., Qian, B., Wang, X.R., Zhong, W.L., Qin, Y., Zhang, H., Gao, W.F., Lei, Y.Y., et al. (2018). Twist1 regulates vimentin through Cul2 circular RNA to promote EMT in hepatocellular carcinoma. Cancer Res. 78, 4150–4162. https://doi.org/10.1158/0008-5472.can-17-3009.

16. Fornes, O., Castro-Mondragon, J.A., Khan, A., van der Lee, R., Zhang, X., Richmond, P.A., Modi, B.P., Correard, S., Gheorghe, M., Baranašić, D., et al. (2020). JASPAR 2020: update of the open-access database of transcription factor binding profiles. Nucleic Acids Res. 48, D87–D92. https://doi.org/10.1093/nar/gkz1001.

17. Pan, S., Zhao, X., Shao, C., Fu, B., Huang, Y., Zhang, N., Dou, X., Zhang, Z., Qiu, Y., Wang, R., et al. (2021). STIM1 promotes angiogenesis by reducing exosomal miR-145 in breast cancer MDA-MB-231 cells. Cell Death Dis. 12, 38. https://doi.org/10.1038/s41419-020-03304-0.

18. Moya, I., Umans, L., Maas, E., Pereira, P., Beets, K., Francis, A., Sents, W., Robertson, E., Mummery, C., Huylebroeck, D., and Zwijsen, A. (2012). Stalk cell phenotype depends on integration of Notch and Smad1/5 signaling cascades. Develop. Cel. 22, 501–514. https://doi.org/10.1016/j.devcel.2012.01.007.

19. Bertero, A., and Murry, C.E. (2018). Hallmarks of cardiac regeneration. Nat. Rev. Cardiol. 15, 579–580. https://doi.org/10.1038/s41569-018-0079-8.

20. Ingason, A.B., Goldstone, A.B., Paulsen, M.J., Thakore, A.D., Truong, V.N., Edwards, B.B., Eskandari, A., Bollig, T., Steele, A.N., and Woo, Y.J. (2018). Angiogenesis precedes cardiomyocyte migration in regenerating mammalian hearts. J. Thorac. Cardiovasc. Surg. 155, 1118–1127.e1. https://doi.org/10.1016/j.jtcvs.2017.08.127.

21. Jeck, W.R., and Sharpless, N.E. (2014). Detecting and characterizing circular RNAs. Nat. Biotechnol. 32, 453–461. https://doi.org/10.1038/nbt.2890.

22. Garikipati, V.N.S., Verma, S.K., Cheng, Z., Liang, D., Truongcao, M.M., Cimini, M., Yue, Y., Huang, G., Wang, C., Benedict, C., et al. (2019). Circular RNA CircFndc3b modulates cardiac repair after myocardial infarction via FUS/VEGF-A axis. Nat. Commun. 10, 4317. https://doi.org/10.1038/s41467-019-11777-7.

23. Zheng, X., Huang, M., Xing, L., Yang, R., Wang, X., Jiang, R., Zhang, L., and Chen, J. (2020). The circRNA circSEPT9 mediated by E2F1 and EIF4A3 facilitates the carcinogenesis and development of triple-negative breast cancer. Mol. Cancer 19, 73. https://doi.org/10.1186/s12943-020-01183-9.

24. Yu, W., Huang, X., Tian, X., Zhang, H., He, L., Wang, Y., Nie, Y., Hu, S., Lin, Z., Zhou, B., et al. (2016). GATA4 regulates Fgf16 to promote heart repair after injury. Development 143, 936–949. https://doi.org/10.1242/dev.130971.

25. Välimäki, M.J., and Ruskoaho, H.J. (2020). Targeting GATA4 for cardiac repair. IUBMB Life 72, 68–79. https://doi.org/10.1002/iub.2150.

26. Liu, G., Huang, K., Jie, Z., Wu, Y., Chen, J., Chen, Z., Fang, X., and Shen, S. (2018). CircFAT1 sponges miR-375 to promote the expression of Yes-associated protein 1 in osteosarcoma cells. Mol. Cancer 17, 170. https://doi.org/10.1186/s12943-018-0917-7.

27. Tzavlaki, K., and Moustakas, A. (2020). TGF-β signaling. Biomolecules 10, 487. https://doi.org/10.3390/biom10030487.

28. Benn, A., Hiepen, C., Osterland, M., Schütte, C., Zwijsen, A., and Knaus, P. (2017). Role of bone morphogenetic proteins in sprouting angiogenesis: differential BMP receptor-dependent signaling pathways balance stalk tip cell competence. FASEB J. 31, 4720–4733. https://doi.org/10.1096/fj.201700193rr.

29. Seystahl, K., Tritschler, I., Szabo, E., Tabatabai, G., and Weller, M. (2015). Differential regulation of TGF-β-induced, ALK-5-mediated VEGF release by SMAD2/3 versus SMAD1/5/8 signaling in glioblastoma. Neuro Oncol. *17*, 254–265. https://doi.org/10.1093/neuonc/nou218.

30. Zhu, Q., Kim, Y.H., Wang, D., Oh, S.P., and Luo, K. (2013). SnoN facilitates ALK1-Smad1/5 signaling during embryonic angiogenesis. J. Cell Biol. *202*, 937–950. https://doi.org/10.1083/jcb.201208113.

31. Benn, A., Alonso, F., Mangelschots, J., Génot, E., Lox, M., and Zwijsen, A. (2020). BMP-SMAD1/5 signaling regulates retinal vascular development. Biomolecules *10*, 488. https://doi.org/10.3390/biom10030488.

32. Wang, Y., Zhao, R., Shen, C., Liu, W., Yuan, J., Li, C., Deng, W., Wang, Z., Zhang, W., Ge, J., and Shi, B. (2020). Exosomal CircHIPK3 released from hypoxia-induced cardiomyocytes regulates cardiac angiogenesis after myocardial infarction. Oxid. Med. Cell. Longev. *2020*, 8418407. https://doi.org/10.1155/2020/8418407.